Available online at www.sciencedirect.com
SCIENCE DIRECT®
Geochimica et Cosmochimica Acta 70 (2006) 2562–2576
Geochimica
www.elsevier.com/locate/gca

Part II. Evaluation of ^{40}Ar–^{39}Ar quartz ages: Implications for fluid inclusion retentivity and determination of initial $^{40}Ar/^{36}Ar$ values in Proterozoic samples

M.A. Kendrick *, J.McL. Miller, D. Phillips

Predictive Mineral Discovery CRC, School of Earth Sciences, University of Melbourne, Vic. 3010, Australia

Received 7 February 2005; accepted in revised form 22 December 2005

Abstract

The argon isotope systematics of vein-quartz samples with two different K-reservoirs have been evaluated in detail. Potassium is hosted by ultra-high-salinity fluid inclusions in quartz samples from the Eloise and Osborne iron-oxide-copper-gold (IOCG) deposits of the Mt Isa Inlier, Australia. In contrast, K is hosted by accidentally trapped mica within lower-salinity fluid inclusions of a sample selected from the Railway Fault, 13 km south of the Mt Isa copper mine, Australia. Imprecise apparent ages have been obtained for all of the samples studied and conclusively demonstrate that quartz fluid inclusions are retentive to Ar and have not leaked over billions of years. IOCG samples that host K in fluid inclusions only, have K/Cl values of <1 and the ages obtained represent the maximum ages for mineralization. In contrast, the Railway Fault samples that include accidentally trapped mica have K/Cl values of ≫1. Excess $^{40}Ar_E$ plus Cl hosted by fluid inclusions, and radiogenic $^{40}Ar_R$ plus K, are strongly correlated in these samples and define a plane in 3D ^{40}Ar–^{36}Ar–K–Cl space. In this case, the plane yields an 'excess $^{40}Ar_E$' corrected age of ~1030 Ma that is 100's of Ma younger than nearby Cu-mineralization at Mt Isa. The age is interpreted to reflect ^{40}Ar-loss from the accidentally trapped mica into the surrounding fluid inclusions, and is not related to the samples' age of formation. The initial $^{40}Ar/^{36}Ar$ value of fluid inclusions is widely used to provide information on fluid origin. For the IOCG samples that host K in fluid inclusions only, the initial $^{40}Ar/^{36}Ar$ values are close to the measured values at every temperature of stepped heating experiments. For samples that include accidentally trapped mica, the correction for post-entrapment radiogenic $^{40}Ar_R$ production is significant. Furthermore, because $^{39}Ar_K$ present in accidentally trapped mica crystals is released at different temperatures to radiogenic $^{40}Ar_R$ lost to the surrounding fluid inclusions, intra-sample $^{40}Ar/^{36}Ar$ variation cannot be reliably documented. The results demonstrate that noble gas analysis is readily applicable to Proterozoic, or older, samples but that if K-mineral impurities are present within quartz the abundance of K must be determined before calculation of mean $^{40}Ar/^{36}Ar$ values that are representative of the samples' initial composition.

1. Introduction

Age constraints on many classes of ore deposit have traditionally been limited by the low abundance of radioactive parent elements in most ore minerals. However, direct dating of hydrothermal phases via solid or fluid inclusions has enabled several previously problematic classes of ore deposit to be dated. Variably successful dating methods include: Ar–Ar quartz (Kelley et al., 1986; Turner and Bannon, 1992; McKee et al., 1993; Qiu, 1996; Kendrick et al., 2001a; Qiu et al., 2002), Ar–Ar pyrite (York et al., 1982; Smith et al., 2001; Phillips and Miller, 2006), Rb–Sr sphalerite (Nakai et al., 1990, 1993; Brannon et al., 1992), Rb–Sr quartz (Shepherd and Darbyshire, 1981; Darbyshire and Shepherd, 1985; Pettke and Diamond, 1995) and U/Th-Pb Calcite (Coveney et al., 2000).

Additionally, the Ar-isotope composition of fluid inclusions in quartz provides constraint on fluid origins and is in many cases of equal interest to sample age (Kelley et al., 1986; Turner and Bannon, 1992; Kendrick et al., 2001b).

* Corresponding author. Fax: +61 3 8344 7761.
E-mail address: mark.kendrick@unimelb.edu.au (M.A. Kendrick).

0016-7037/$ - see front matter © 2006 Elsevier Inc. All rights reserved.
doi:10.1016/j.gca.2005.12.024

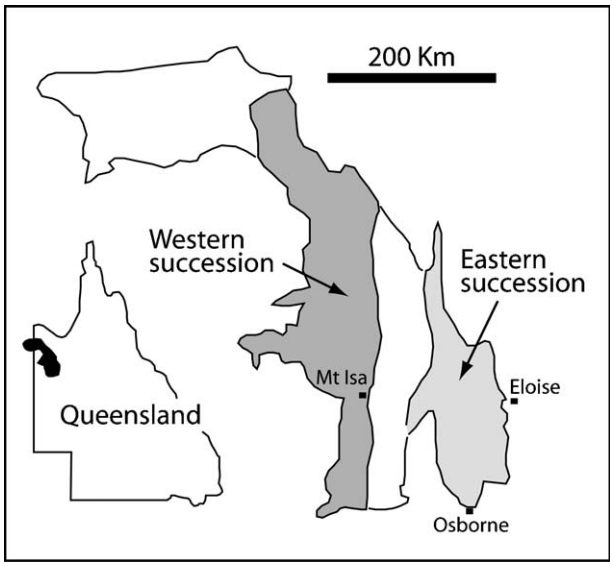

Fig. 1. Locality map indicating the position of the Mt Isa Inlier within western Queensland, northeast Australia, and the location of Eloise and Osborne plus Mt Isa, 13 km north of the Railway Fault sample locality.

For example, initial $^{40}Ar/^{36}Ar$ values vary by orders of magnitude and can be used to distinguish meteoric water, with values of ~296, from deep crust or mantle fluids with values of >10,000 (e.g., MORB value >40,000; Burnard et al., 1997).

Successful determination of either an Ar–Ar quartz age or the initial $^{40}Ar/^{36}Ar$ value depends upon deconvolution of three ^{40}Ar components: (1) post-entrapment radiogenic $^{40}Ar_R$, formed in situ by the radioactive decay of ^{40}K, and ^{40}Ar present in the fluid inclusion at the time of trapping with an (2) atmospheric $^{40}Ar_A$ ($296 \times {}^{36}Ar_A$) or (3) excess $^{40}Ar_E$ origin.[1] If the sample age is known, the initial $^{40}Ar/^{36}Ar$ value is easily determined from the measured $^{40}Ar/^{36}Ar$ value and K content measured as $^{39}Ar_K$. However, the prevalence of excess $^{40}Ar_E$ in fluid inclusions, provides a significant challenge to Ar–Ar age determination (Rama et al., 1965). The problem has previously been overcome through the use of isochron diagrams (McKee et al., 1993; Qiu, 1996; Qiu et al., 2002), or 3D multi-component correlation diagrams (Kelley et al., 1986; Turner and Bannon, 1992; Kendrick et al., 2001a).

In the present study, we examine the proportion of radiogenic $^{40}Ar_R$ to that of the initial component ($^{40}Ar_E + {}^{40}Ar_A$) in six samples collected from the Mt Isa Inlier, northeast Australia (Fig. 1). This was undertaken to test how susceptible Proterozoic quartz samples will be to distortions in the initial $^{40}Ar/^{36}Ar$ values caused by $^{40}Ar_R$ ingrowth. Furthermore, we examine the use of isochron and 3D multi-component correlation diagrams and evaluate why different noble gas extraction techniques have been variably successful in Ar–Ar age determination of quartz.

[1] Excess $^{40}Ar_E = {}^{40}Ar$ not sourced from the atmosphere or by radiogenic decay of ^{40}K. $^{40}Ar_E = {}^{40}Ar_{total} - {}^{40}Ar_R - {}^{40}Ar_A$.

2. Samples and methodology

2.1. Fluid inclusions

The origin of the samples is summarized in Table 1. Fluid inclusions from these samples have been analysed by microthermometry and are described in detail in Part I (Kendrick et al., 2006). The IOCG samples from Eloise and Osborne include predominantly primary ultra-high-salinity multi-solid (MS), liquid–vapour–daughter (LVD) and lower-salinity, predominantly secondary, liquid–vapour (LV), monophase (M) and carbon-dioxide (CO_2) fluid inclusions. Potassium is present in solution and in sylvite daughter minerals.

Sample AW02-002 from the Railway Fault includes primary liquid–vapour fluid inclusions that define growth zones and include accidentally trapped mica (Fig. 2). The mica was not visible optically but has been imaged by electron microscopy (Figs. 1b versus d–f). The sample Ar, K and Cl abundances are summarized in Table 2 and indicate that the accidentally trapped mica (Figs. 2d–f) fills an average of ~50% of the fluid inclusions volume. This and the sample K/Cl values of $\gg 1$ indicate that the accidentally trapped mica is the major reservoir of K in this sample.

2.2. Irradiation and mass spectrometry

The analytical protocol has been described in detail in Part I (Kendrick et al., 2006). Sample gas was extracted from fluid inclusions in quartz vein samples by stepped heating. In addition, duplicate analyses of samples AW02-002b and EL 48177 were obtained by combined in vacuo crushing and stepped heating of the crushed residue.

The Ar isotopic composition of purified noble gas was measured utilizing the MAP 215-50 (Mass Analyser Products) noble gas mass spectrometer at the University of Melbourne. The samples were irradiated for 150 MWH in position 5c of the McMaster reactor and received a total neutron fluence of $\sim 10^{19}$ neutrons cm^{-2}. The irradiation parameters determined from Hb3Gr and GA1550 monitors are given in Part I (Kendrick et al., 2006). Standard corrections have been made for Ar-interference reactions, mass discrimination and decay of ^{37}Ar and ^{36}Cl since the time of irradiation. The molar abundances of K, Cl and Ca are calculated from the irradiation parameters J, β and α using the noble gas proxies $^{39}Ar_K$, $^{38}Ar_{Cl}$ and $^{37}Ar_{Ca}$ (Kendrick et al., 2006).

3. Age determinations

3.1. Osborne

Stepped heating analyses were conducted on two Osborne samples, OS 37A and OS 37B. Data points from the samples exhibit a weak correlation in 3D ^{40}Ar–K–Cl–^{36}Ar space with one distinct outlier (Fig. 3a). The weak correlation between $^{40}Ar/^{36}Ar$ and $K/^{36}Ar$ is also apparent

Table 1
Sample material

Sample	Description	Location
Eloise		
EL 48179 EL 48177	Quartz vein samples with populations of multiple fluid inclusion types. Described in detail by Baker (1998)	Drill holes— END39, 311.1m 145B/END35C/290m
Osborne		
OS 37A OS 37B	Quartz veins with po-py-cpy-mag-bio (dominantly infill (37A)) and mag-py-cpy (dominantly magnetite with less abundant infill texture (37B))	Drill hole— TTNQ260/220-220.19m/3E ore body
Railway Fault		
AW02-002a AW02-002b OS37B	Two separates from one quartz vein hand specimen Quartz zoning is defined by Cu-rich primary two-phase liquid-vapour fluid inclusions	GR 344770 7694060 13 km south of the Mt Isa Cu mine

The Eloise, Osborne and Railway Fault samples where provided by T. Baker, R. Mustard and A. Wilde, respectively. The fluid inclusion assemblages are described in detail in Part I (Kendrick et al., 2006).

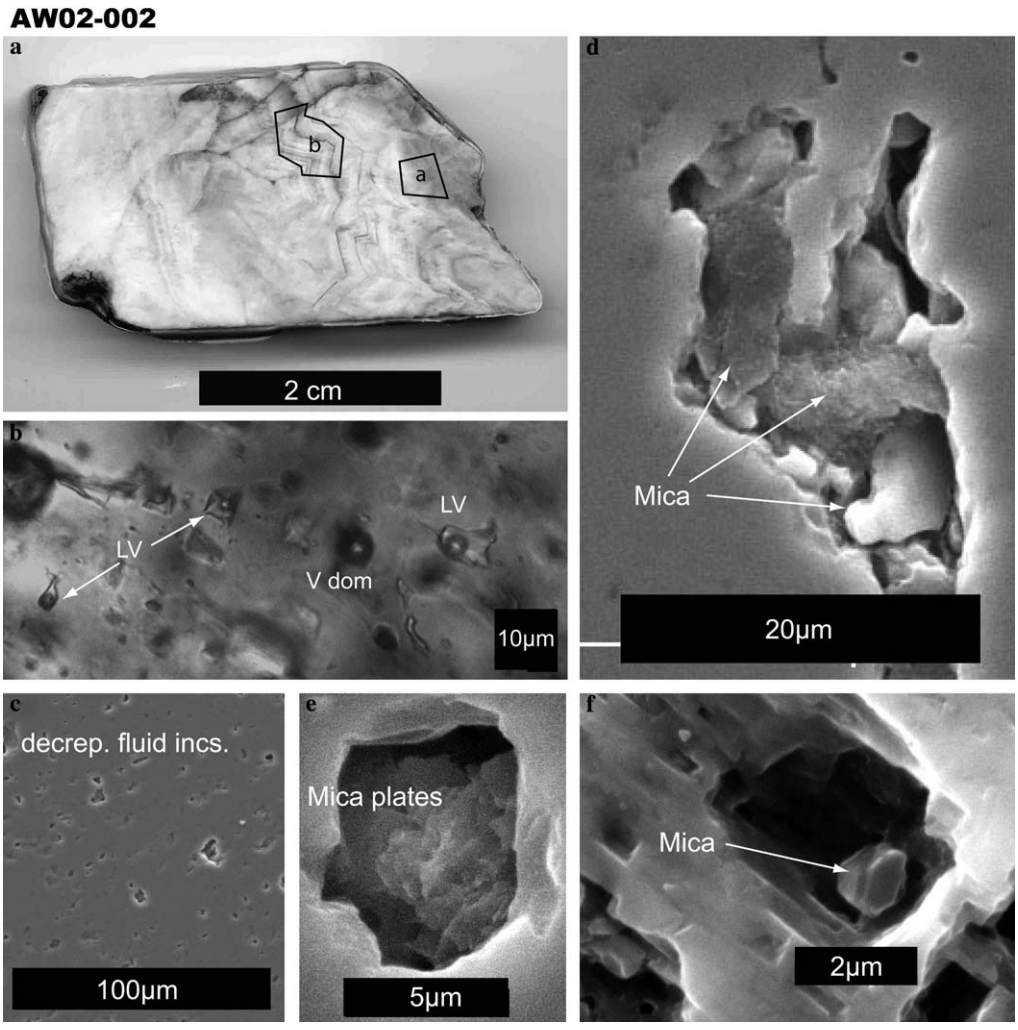

Fig. 2. Sample AW02-002 from the Railway Fault. (a) Photograph of the hand specimen indicating the positions of the splits AW02-002a and AW02-002b. Note zoning defined by primary fluid inclusions. (b) Optical microscopic image of two-phase liquid–vapour fluid inclusions. Solid daughter minerals or accidentally trapped mica were not observed in any of the fluid inclusions (see also Kendrick et al., 2006, Part I). (c–f) Secondary electron micrographs. Fluid inclusions are observed as craters/pits in the gold coated polished surface of the sample. Platy mica crystals are clearly observed in (d) and (e), and possibly in (f). These crystals were confirmed as K–Al-silicates by the energy dispersive X-ray detector of the SEM.

in a conventional 2D isochron (Fig. 3b). Although a regression can be forced through selected data points, the uncertainty is improved by assuming an atmospheric intercept and calculating apparent ages for individual heating steps (Fig. 3b). The slope defined by the data point with the youngest apparent age of 1630 ± 89 Ma is shown in

Table 2
Determination of impurity characteristics from argon–argon K–Cl data[a] and fluid inclusion characteristics

Quartz sample Name	Mass (mg)	Vol[b] (mm^3)	FI + Matrix				Fluid inclusions (FI)		FI[d] (mm^3)	Vol % FI	Impurities		Max fill of musc in FI %[f]
			K/Cl (molar)	K (ppm)	Cl (ppm)	Ar (ppb)	NaCl eq[c] Wt %	% V Fill[c]			Musc[e] (mm^3)	Vol % musc	
Eloise													
EL 48177	22.5	8.5	0.06	40	655	10	30 ± 10	15 ± 10	0.09 ± 0.02	1.0 ± 0.2			
EL 48177	26.0	9.8	0.05	31	549	7	30 ± 10	15 ± 10	0.08 ± 0.02	0.8 ± 0.2			
EL 48179	92.0	34.7	0.05	9	154	3	25 ± 15	15 ± 10	0.10 ± 0.03	0.3 ± 0.1			
Osborne													
OS37A	41.9	15.8	0.28	12	39	2	25 ± 10	15 ± 10	0.012 ± 0.003	0.07 ± 0.02	Minor?		
OS37B	43.2	16.3	0.12	27	200	1	45 ± 15	15 ± 10	0.04 ± 0.01	0.3 ± 0.1			
Railway Fault													
AW02-002a	126	47.5	8.63	819	86	41	12 ± 5	50 ± 30	0.32 ± 0.14	0.7 ± 0.3	0.37	0.77	53 ± 24
AW02-002b	22.9	8.6	7.00	726	94	34	12 ± 5	50 ± 30	0.06 ± 0.03	0.7 ± 0.3	0.06	0.68	48 ± 23
AW02-002b	23.3	8.8	7.00	591	77	27	12 ± 5	50 ± 30	0.05 ± 0.02	0.6 ± 0.3	0.05	0.56	48 ± 23

[a] Full data set available in Appendix A.
[b] Sample volume calculated assuming the density of quartz 2.65 g cm^{-3}.
[c] A large uncertainty is assigned to reflect the range of fluid inclusion types.
[d] The total fluid inclusion volume is calculated from the sample Cl abundance, the fluid inclusion salinity, degree of fill and by assuming all Cl is present within the fluid inclusions and the liquid phase has a density of 1 g cm^{-3}.
[e] Where present the volume of accidentally trapped mica has been calculated based on the sample K abundance, the chemical formula and density (2.88 g cm^{-3}) of muscovite and the assumption that all K is hosted by the mica impurity.
[f] The % fill of accidentally trapped mica in the fluid inclusions = (musc vol)/(musc + FI vol). The uncertainty is due to the variable fill and salinity of the fluid inclusions. The figure represents an upper limit because the volume of mica will have been slightly over estimated if significant K is present as a solute within the fluid inclusions.

Fig. 3b. A significant proportion of heating steps exhibit apparent ages within error of this result, as indicated by the proximity of most data points to the reference line (Fig. 3b) and by the age spectrum plot (Fig. 3c).

The youngest apparent age of 1630 ± 89 Ma age determined for Osborne has a low precision of 5%, but is close to the Re–Os molybdenite, U–Pb titanite and Ar–Ar metamorphic biotite ages of 1595–1600 Ma that are considered to constrain the syn-D_2 mineralisation event (Perkins and Wyborn, 1998; Gauthier et al., 2001; Rubenach et al., 2001; Giles and Nutman, 2002). The precision of only 5% means it is also just within error of previous Ar–Ar hydrothermal biotite ages of ~1540 Ma (Perkins and Wyborn, 1998) that may constrain a later retrograde-hydrothermal-event (Gauthier et al., 2001; Rubenach et al., 2001) or be explained as cooling ages.

3.2. Eloise

Stepped heating analyses were conducted on two Eloise samples EL 48177 and EL 48179. In addition a second split of sample EL 48177 was analysed by combined in vacuo crushing and stepped heating of the crushed residue. Data from the uncrushed samples are very weakly correlated in 3D ^{40}Ar–K–Cl–^{36}Ar space (Fig. 3d), but it is clearly seen on the 2D isochron diagram that the majority of data points lie close to the $^{40}Ar/^{36}Ar$ axis indicating that they are dominated by excess $^{40}Ar_E$ (Fig. 3e). A mixing line could be drawn through these data points, but it has an almost vertical trajectory and no age significance (Fig. 3e). The lack of a good K–$^{40}Ar_R$ correlation is despite a mean fluid inclusion salinity of 25–30 wt % NaCl eq and K/Cl values of 0.05–0.3 (Table 2) that indicate fluid inclusion K concentrations of several weight percent.

The youngest apparent age of 1790 ± 270 Ma is too imprecise to provide a useful age constraint, although it is still within error of the deposits preferred age of 1514–1530 Ma (Fig. 3e; Baker et al., 2001). Furthermore, the age is based on a small proportion of the sample gas (9% of EL 48177) and the majority of steps have apparent ages older than the Earth (Appendix A).

In contrast to results from the uncrushed samples, heating steps obtained from the crushed residue of sample EL 48177 are strongly correlated in $K/^{36}Ar$ versus $^{40}Ar/^{36}Ar$ space (Fig. 3f). Although the analytical uncertainty on individual steps is large (due to small gas volumes in these steps) a regression forced through selected data points yields an age of 1542 ± 266 Ma (Fig. 5f). This age remains imprecise but is almost identical to the preferred mineralization age of 1514–1530 Ma determined from hydrothermal biotite (Baker et al., 2001). It has a non-atmospheric initial $^{40}Ar/^{36}Ar$ value of ~735 that is realistic for the sample (Fig. 3f).

It is well documented that in vacuo crushing preferentially samples fluid inclusions and can allow an improved age determination by stepped heating the remaining K-mineral impurities within crushed quartz samples (Turner and Bannon, 1992; Kendrick et al., 2001a). However, even the most K-rich heating steps in Fig. 3f have K/Cl values of ⩽0.35. This value is realistic for K-rich primary fluid inclusions and indicates that significant mineral impurities are not present in the sample. Instead, the improved isochron, obtained from the crushed sample can be explained if in vacuo crushing has preferentially decrepitated secondary fluid inclusions

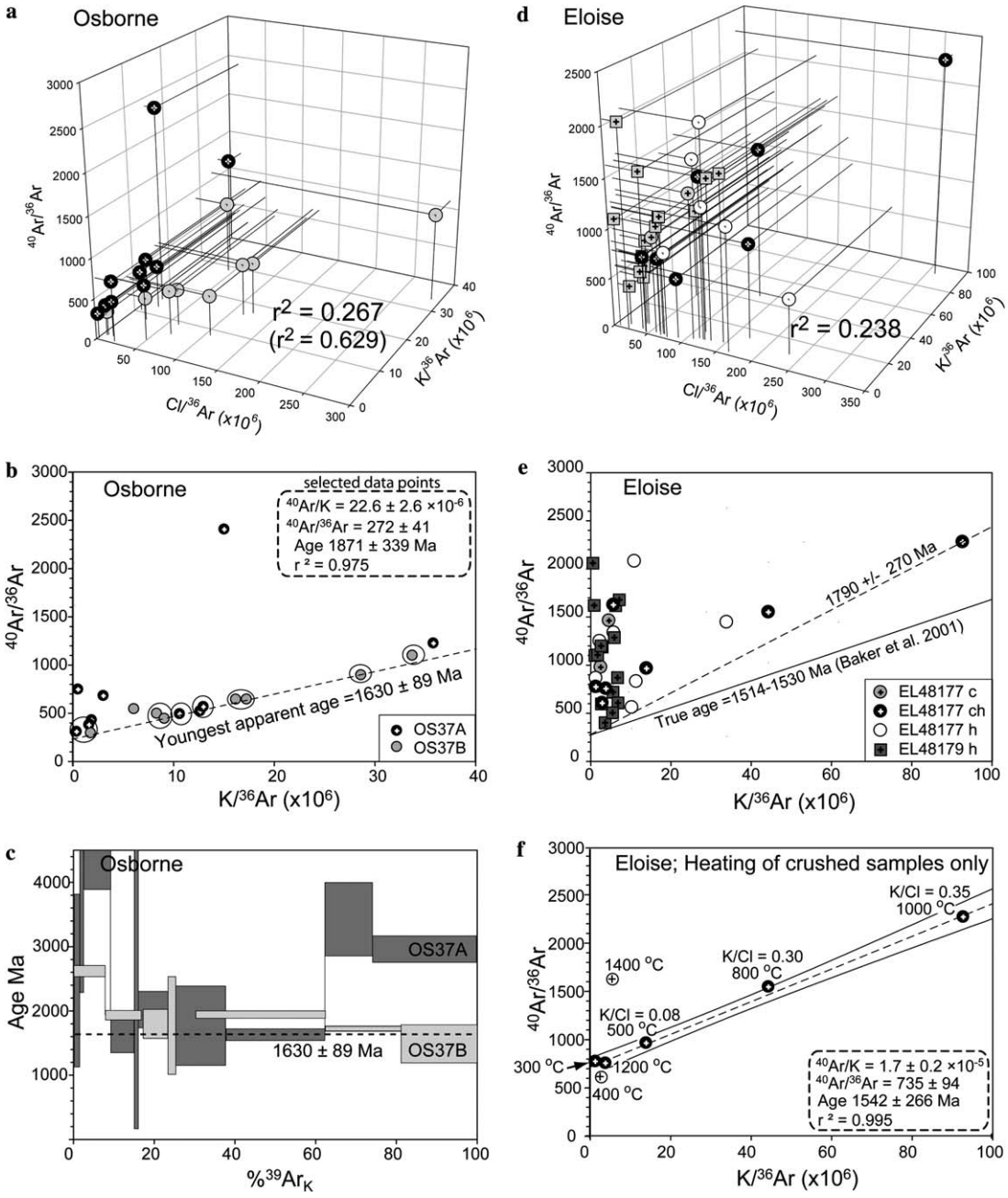

Fig. 3. Age constraints on the Osborne and Eloise IOCG deposits of the Eastern Succession. (a) 3D ^{40}Ar–K–Cl–^{36}Ar multi-component correlation diagram for Osborne. The correlation coefficient is shown for all the data points and in brackets with the outlier omitted. (b) 2D isochron plot for Osborne showing the youngest apparent age of an individual step and the statistics for the best regression that can be obtained for selected datapoints. (c) Age spectrum plot for the Osborne samples. (d) 3D ^{40}Ar–K–Cl–^{36}Ar multi-component correlation diagram for Eloise. (e) 2D isochron plot for Eloise, showing the youngest apparent age obtained for an individual heating step. (f) Isochron regression for the crushed residue of sample EL 48177. nb—Regressions in (b) and (f) have been obtained by weighting each data pointed equally and disregarding analytical uncertainty (model 2, isoplot) so MSWD values are not given.

that lie along planes of weakness. The crushed residue would then be enriched in primary fluid inclusions that have a more uniform initial $^{40}Ar/^{36}Ar$ composition (Fig. 3f).

3.3. The Railway Fault

Sample AW02-002 exhibits a strong correlation between ^{40}Ar, K and Cl in 3D ^{40}Ar–K–Cl–^{36}Ar space (Figs. 4a and b). As in previous studies the mixing-planes are defined by three components (Kelley et al., 1986; Turner and Bannon, 1992; Kendrick et al., 2001a); (1) atmospheric $^{40}Ar_A$ and ^{36}Ar with a $^{40}Ar/^{36}Ar$ intercept of 295.5; (2) Cl-correlated fluid inclusion ^{40}Ar and (3) K-correlated radiogenic $^{40}Ar_R$ produced in situ within accidentally trapped mica-crystals (Fig. 4).

The 3D isochron regressions represent much improved data fits compared to the 2D isochrons, with respective MSWD values of <30 versus >1000 (Fig. 4). The two splits

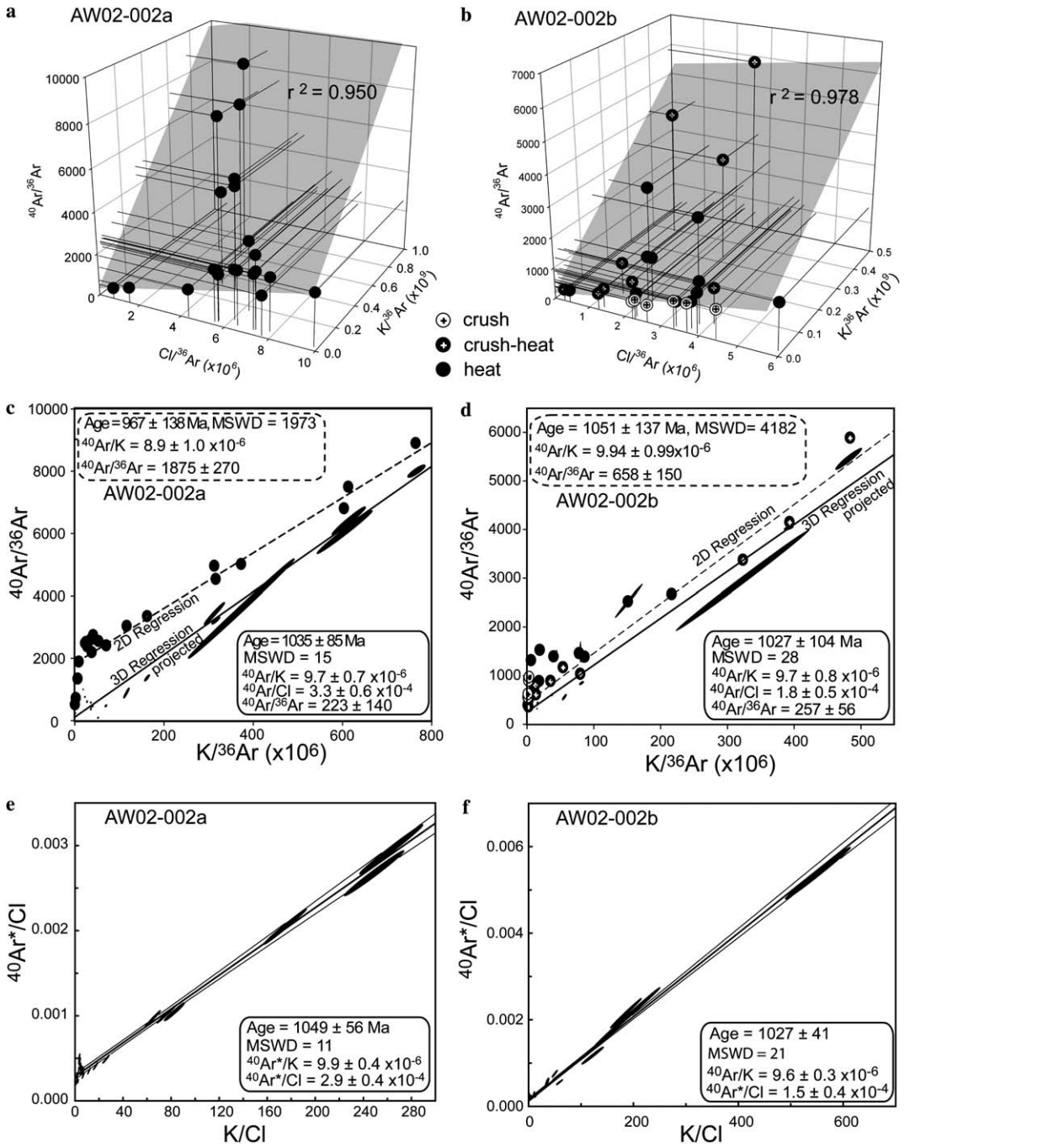

Fig. 4. Age constraints on samples AW02-002a and AW02-002b from the Railway Fault. (a and b) Stepped heating only and combined in vacuo crushing plus stepped heating data define planes in 3D ^{40}Ar–K–Cl–^{36}Ar space. (c and d) The data are shown as circles on standard 2D isochron diagrams a regression through this data and the corresponding statistics are identified by dashed lines. In addition, correlated error ellipses are shown for the data projected down the slope of the 3D planes (in a and b), the 3D regression and statistics are identified by solid lines. (e and f) The atmospheric component is absent in $^{40}Ar^*$/Cl–K/Cl diagrams and the regression line represents mixing between the Cl-dominated fluid inclusions and K-rich accidentally trapped mica component. $^{40}Ar^* = {}^{40}Ar_R + {}^{40}Ar_E$ (or $^{40}Ar_{total} - {}^{36}Ar \times 295.5$).

of sample AW02-002 exhibit significant ($t = 0$) interzonal variation in isotopic composition. The 2D isochron $^{40}Ar/^{36}Ar$ intercepts of 1875 ± 270 plus 658 ± 150 and the 3D isochron $^{40}Ar/Cl$ slopes of 3.3×10^{-4} and 1.8×10^{-4} are significantly different for AW02-002a and AW02-002b (Figs. 2a–d). Whereas the $^{40}Ar_R/K$ slopes obtained from the 2D and 3D isochrons define fairly imprecise (~10%) but within error ages.

The best data fit is obtained from K/Cl versus $^{40}Ar/Cl$ plots (Turner and Bannon, 1992) that have MSWD values of just 11 and 21. These plots are advantageous because both ratios are free of atmospheric $^{40}Ar_A$, meaning the three component mixture can be presented in 2D (Figs. 3e and f). The $^{40}Ar/Cl$ intercepts obtained from these regressions are within error of the values determined from the 3D isochron slopes (compare Figs. 4a,b with e,f). The

quality of fit is however still limited by the variable Ar-isotope composition of fluid inclusions in different zones of the sample. Nonetheless, the apparent ages of AW02-002a and AW02-002b are indistinguishable at 1049 ± 56 Ma and 1027 ± 41 Ma (Figs. 4e and f) and the most precise age of 1027 ± 41 Ma has uncertainty at the 4% level.

The above apparent ages are 100's of Ma younger than the preferred ~1523 Ma age of Cu-mineralization at the nearby Mt Isa mine, that has been constrained by textural relationships, Ar–Ar biotite ages and Pb-isotope data (Swager, 1985; Perkins et al., 1999; Carr et al., 2004). It is possible that the Railway Fault is unrelated to mineralization at Mt Isa, and that the ~1030 Ma age represents the time of movement on this fault. However, an alternative explanation for the discrepancy is examined below.

4. Significance of ages

4.1. Quartz fluid inclusion ages

The samples from Eloise and Osborne have mean K/Cl values of <0.3 (Table 2), suggesting that significant mica impurities are absent and that K is sited in the fluid inclusions of these samples.

The youngest apparent ages determined from these samples, are within error of the preferred ages for the two deposits. Therefore, the data confirm that the fluid inclusions have not leaked since the time of trapping 1.5–1.6 Ga ago. However, robust isochron regressions were not obtained from these samples, and the apparent ages are calculated assuming an atmospheric initial $^{40}Ar/^{36}Ar$ value. If excess $^{40}Ar_E$ was present the ages will have been overestimated and are therefore interpreted as maximum ages for mineralisation. The assumption of an atmospheric intercept appears to be reasonable for the Osborne samples, where an intercept within error of the atmospheric value is obtained by regression of selected data points (Fig. 3b). However, the presence of significant quantities of excess $^{40}Ar_E$ in the Eloise samples mean that even the youngest apparent age is elevated above the preferred value (Fig. 3e).

4.1.1. Secondary fluid inclusions and mixing

The IOCG samples contain multiple types of fluid inclusions with secondary LV fluid inclusions dominating in some samples (Part I; Kendrick et al., 2006). In the case of the Osborne samples, the proximity of most data points to the youngest age of 1630 ± 89 Ma (Fig. 3b), suggests that the secondary fluid inclusions must have been trapped during or soon after mineralization. The isochron obtained for the crushed residue of the Eloise sample EL 48177 (Fig. 3f) was explained by suggesting that in vacuo crushing preferentially removes secondary fluid inclusions.

We now examine the possibility that the above 'isochron' ages (Figs. 3b and f) could be mixing lines caused by mixing of different types of contemporaneous fluid inclusion. Mixing lines that are younger than the sample will have elevated $^{40}Ar/^{36}Ar$ intercepts and mixing lines that are older than the sample will have low $^{40}Ar/^{36}Ar$ intercepts (Fig. 5). As the minimum possible intercept value is the atmospheric $^{40}Ar/^{36}Ar$ value of 296, this places a restriction on the range of compositions and apparent ages that can be obtained by mixing scenarios.

(1) Interpretation of the 1630 ± 89 Ma age obtained for Osborne as the maximum mineralisation age is not affected by possible mixing scenarios because this age was calculated by assuming an atmospheric intercept that represents the minimum value possible. It was demonstrated in Part I that different fluid inclusion types decrepitate at different temperatures (Kendrick et al., 2006), compatible with the $K/^{36}Ar$-variation seen in the isochron diagram (Fig. 3b). Therefore, the proximity of most data points to the 1630 Ma reference line (Fig. 3b) suggests that mixing has occurred between different fluid inclusions with similar initial

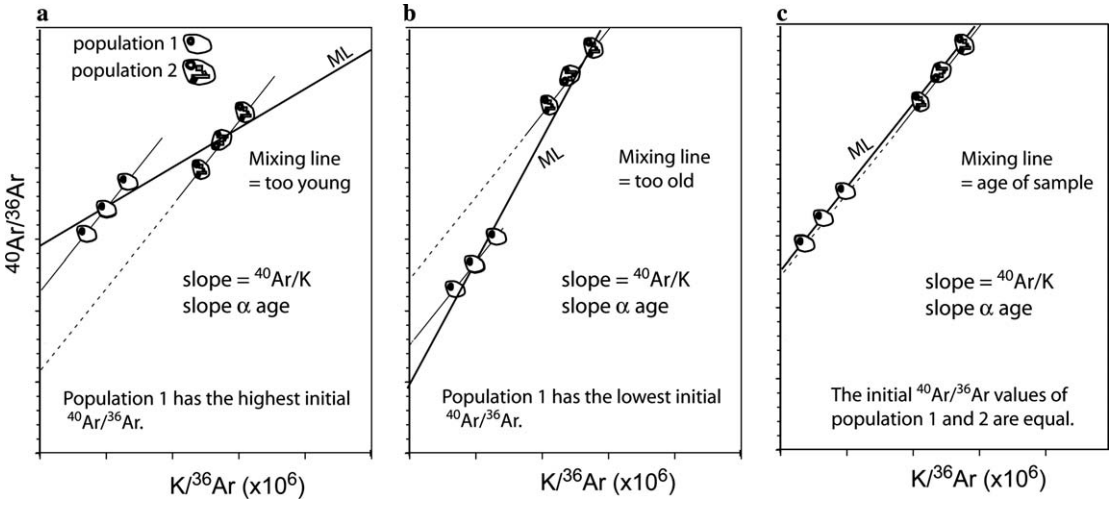

Fig. 5. Possible fluid inclusion mixing scenarios in samples with complex fluid inclusion assemblages. (a) Mixing resulting in a young age. (b) Mixing resulting in an old age. (c) mixing does not influence the age if the different fluid inclusion types have similar initial $^{40}Ar/^{36}Ar$ values. ML, mixing line.

$^{40}Ar/^{36}Ar$ values of close to 296 (Fig. 5c). The few outlying points seen in the 3D plot and the 2D isochron must represent additional fluid inclusion populations with higher initial $^{40}Ar/^{36}Ar$ values.

(2) The Eloise samples exhibit greater spread in $^{40}Ar/^{36}Ar$ values and the data is not correlated in $^{40}Ar/^{36}Ar$ versus $K/^{36}Ar$ space (Figs. 3d and e). This is compatible with the decrepitation and mixing of different fluid inclusions types with different initial $^{40}Ar/^{36}Ar$ values, but the data clearly do not define a mixing line that could be mistaken for the age of mineralization (Figs. 3d and e). The isochron regression obtained for the crushed residue of sample EL 48177 has a non-atmospheric intercept (Fig. 3f) that yields an (imprecise) age almost identical to the preferred age of mineralization. Therefore this age must also represent mixing of fluid inclusions with similar initial $^{40}Ar/^{36}Ar$ values (Fig. 5c).

In conclusion, although mixing lines are theoretically possible in complex samples containing multiple fluid inclusion types, the samples analysed here, that contain fluid inclusions with variable $^{40}Ar/^{36}Ar$, do not produce mixing lines. The only mixing lines produced are between fluid inclusions with similar initial $^{40}Ar/^{36}Ar$ values (Fig. 5c) that therefore produce ages close to the deposit ages. Mixing does not appear to have been significant for the fluid inclusion ages determined here with precision levels of only 4–5%. Furthermore, the quality of the regression is likely to decrease as increasingly dissimilar fluid types are mixed and it is therefore likely that the precision will decrease to such a level that all mixing ages will remain within error of the true formation age.

4.2. Quartz mineral impurity ages

Sample AW02-002 includes accidentally trapped mica as the major reservoir of K (Fig. 2; Table 1; and Part I Kendrick et al., 2006). Most previous quartz-ages determined on samples that include a mineral impurity, have been close to independently determined mineralization ages or compatible with existing mineralisation models (Kelley et al., 1986; Turner and Bannon, 1992; Kendrick et al., 2001a). Although some of these ages were determined from mineral impurities within the quartz matrix (Kendrick et al., 2001a), rather than accidentally trapped mica within the fluid inclusions (Kelley et al., 1986; Turner and Bannon, 1992), the deposits selected have all been rapidly cooled Phanerozoic magmatic-hydrothermal-systems.

In contrast, sample AW02-002, was collected from close to the Proterozoic Mt Isa copper mineralizing system in an area with a protracted thermal history (Spikings et al., 2002). The age of ~1030 Ma is much younger than expected and does not constrain the time of mineralization at Mt Isa. Although the fluid inclusion ages presented above prove that quartz is retentive to ^{40}Ar, we now examine Ar-remobilisation within sample AW02-002, between the accidentally trapped mica and the surrounding fluid inclusion reservoir.

4.2.1. Intra sample ^{39}Ar-recoil

The production of $^{39}Ar_K$ by the neutron reaction $^{39}K(n,p)\,^{39}Ar$ has a mean recoil energy of 177 keV and results in recoil of $^{39}Ar_K$ over several 100 nm leaving a mean $^{39}Ar_K$ depletion depth of 82 nm in silicate minerals (Turner and Cadogan, 1974; Onstott et al., 1995). By comparison, recoil of $^{38}Ar_{Cl}$ is less energetic and results in a mean depletion depth of only 0.6 nm (Onstott et al., 1995). Recoil-loss of $^{39}Ar_K$ does not appear to be significant for the Osborne or Eloise fluid inclusion ages, because $^{39}Ar_K$ and $^{38}Ar_{Cl}$ are released from the sample simultaneously, indicating that fluid inclusions remain the major reservoir of K, Cl and all Ar-isotopes irrespective of recoil (see Part I; Kendrick et al., 2006).

The accidentally trapped mica in sample AW02-002 has maximum dimensions of a few microns (Fig. 2), but the minimum dimension of these platy crystals could be substantially less than 1 μm. Therefore recoil-loss of $^{39}Ar_K$ is likely and explains the artificially high K/Cl values of 0.7–0.8 determined for fluid inclusions in this sample by in vacuo crushing (Table 4 of Kendrick et al., 2006). Nonetheless, the release systematics of $^{39}Ar_K$ from sample AW02-002 indicate that the accidentally trapped mica remains the predominant reservoir of $^{39}Ar_K$ (94% of $^{39}Ar_K$ was released by stepped heating the crushed residue of AW02-002b compared to only 6% during in vacuo crushing; Kendrick et al., 2006). Furthermore, recoil-loss of $^{39}Ar_K$ leads to elevated apparent ages so cannot explain the younger than expected apparent age of ~1030 Ma obtained for sample AW02-002. Rather it is indicated that thermal loss of $^{40}Ar_R$ from the mica crystals is more significant than $^{39}Ar_K$ recoil-loss.

4.2.2. Intra sample ^{40}Ar-loss

The fluid inclusion homogenization temperatures for sample AW02-002 lie in the range 120–300 °C (Part I; Kendrick et al., 2006) which define the minimum temperature of this sample at the time of fluid trapping. The actual temperature of the fluids at the time of trapping depends on the sample depth, but the maximum temperature of the fluids at Mt Isa is also inferred to be close to 270–350 °C (Heinrich et al., 1989), suggesting that if the samples are related, this is an upper limit.

Analysis by the SEM energy dispersive X-ray detector confirmed the platey crystals observed in Fig. 2 as K–Al-silicate. The mineral is therefore probably muscovite mica which is more commonly trapped in fluid inclusions than biotite. However, biotite cannot be ruled out if Fe and Mg were present but undetected by the electron dispersive analysis. Muscovite and biotite are commonly assigned nominal closure temperatures of 350 and 300 °C, respectively (McDougall and Harrison, 1999). The closure temperature of >10 to ~25 μm captive white mica in rapidly cooled Sn-W related mineralization was estimated as

~350 °C (Kelley et al., 1986). These values are all similar to the fluid trapping temperature of sample AW02-002.

However, closure temperature is a function of not only composition, but also the grain-size plus cooling rate, and the calculated value also depends upon the geometry of the diffusion domain (McDougall and Harrison, 1999) and is reduced further by the presence of fluids in hydrothermal systems (Kent and McCuaig, 1997). The effective closure temperature of the accidentally trapped mica in this study is poorly constrained, but could easily have been as low as 160–200 °C and was almost certainly not higher than 250 °C because: (1) the regional cooling rate may have been as low as 0.2 °C Ma^{-1}, Ar–Ar cooling ages for mica and feldspar indicate cooling from 350 °C at ~1400 Ma to 250 °C at ~800 Ma (Fig. 7; Spikings et al., 2002). (2) Many mica crystals are sub-5 μm and have minimum dimension that are probably less than 1 μm (Fig. 2). (3) An infinite cylinder is a better description of the diffusion domain in muscovite than a plane sheet (Hames and Bowring, 1994). The effect of these three parameters on closure temperature is illustrated in Fig. 6.

The quartz vein age is plotted against the maximum estimated closure temperature on the regional cooling T-t path of Spikings et al. (2002) in Fig. 7. The apparent age and estimated mica closure temperature plot close to the interpreted regional cooling trajectory and are compatible with an interpretation whereby sample AW02-002 formed during regional fluid flow and mineralization at Mt Isa (~1523 Ma; Perkins et al., 1999) and cooled through the

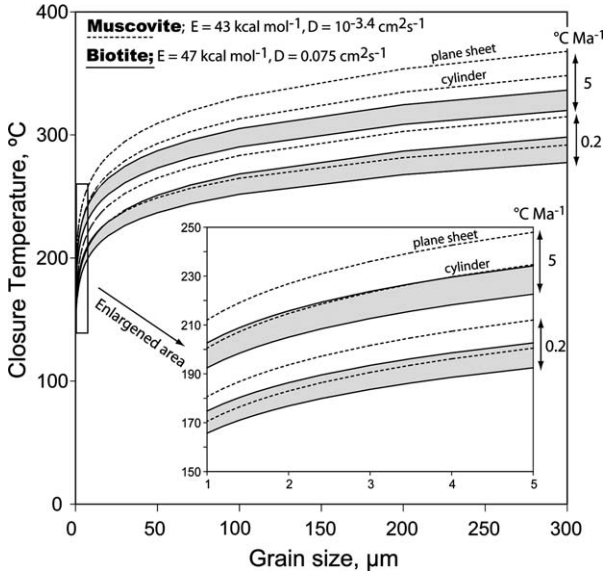

Fig. 6. Closure temperature versus grain size for muscovite and biotite. The top four curves have cooling rates of 5 °C Ma^{-1} and represent; (1) muscovite, plane sheet, (2) muscovite, cylinder, (3) biotite, plane sheet, (4) biotite, cylinder. The bottom four curves represent the same grains cooled at a slower rate of 0.2 °C Ma^{-1}. The curves have been calculated using the closure equation of Dodson (1973) and activation energies (Ea) plus diffusion coefficients (Do) that are considered representative for the Cooma biotite and muscovite (see McDougall and Harrison, 1999).

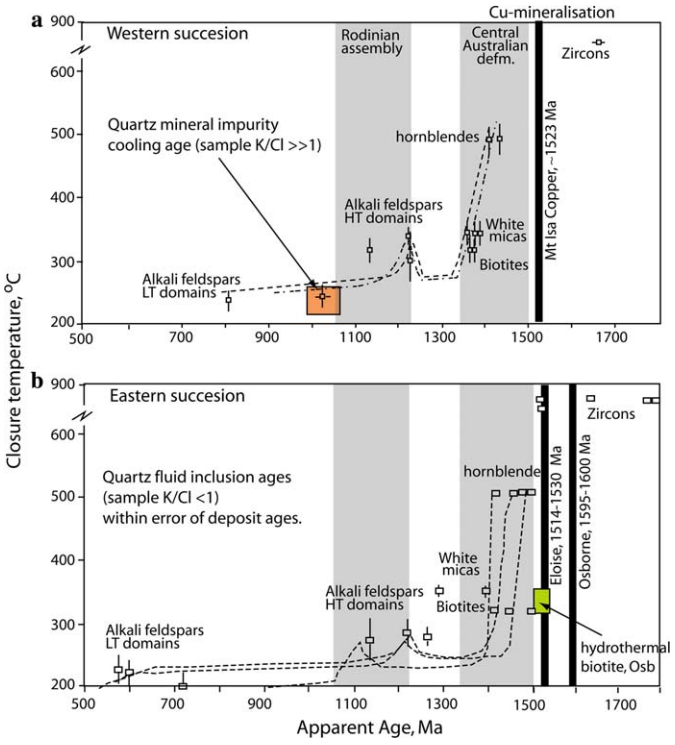

Fig. 7. Interpreted Ar–Ar cooling trajectories for the western (a) and eastern (b) successions of Mt Isa (modified after Spikings et al., 2001, 2002; HT, high temperature; LT, low temperature). (a) The preferred ~1523 Ma biotite age for Mt Isa Cu mineralization (Perkins et al., 1999) and the isochron age of sample AW02-002 together with the maximum closure temperature of sub-5μm mica crystals are shown. (b) The preferred 1595 and 1514–1530 Ma mineralization ages are shown for Osborne and Eloise, respectively (Rubenach et al., 2001; Gauthier et al., 2001; Baker et al., 2001). The younger <1540 Ma hydrothermal biotite age is also shown for Osborne (Perkins and Wyborn, 1998) and may be related to either retrograde hydrothermal overprinting (Rubenach et al., 2001; Gauthier et al., 2001) or biotite closure temperature.

effective closure temperature of variably sized accidentally trapped mica at ~1030 Ma. The intra-sample remobilization of ^{40}Ar in the different samples is summarized graphically in Fig. 8.

5. Implications for noble gas studies

The fluid inclusion results presented above have demonstrated that quartz is retentive to ^{40}Ar over billions of years and that secondary fluid inclusions (in the Osborne samples) formed close to the time of primary fluid inclusion entrapment during mineralization.

In this study it was straightforward to correct the measured $^{40}Ar/^{36}Ar$ value for radiogenic $^{40}Ar_R$ because K was measured as $^{39}Ar_K$ and the Proterozoic mineralization ages are constrained independently (Perkins et al., 1999; Baker et al., 2001; Gauthier et al., 2001). However, many noble gas studies are undertaken on samples that are not irradiated meaning that K is not measured simultaneously, and sometimes the age of mineralization is unknown or uncertain.

The size of the correction for post-entrapment radiogenic $^{40}Ar_R$ production for the IOCG samples from Eloise

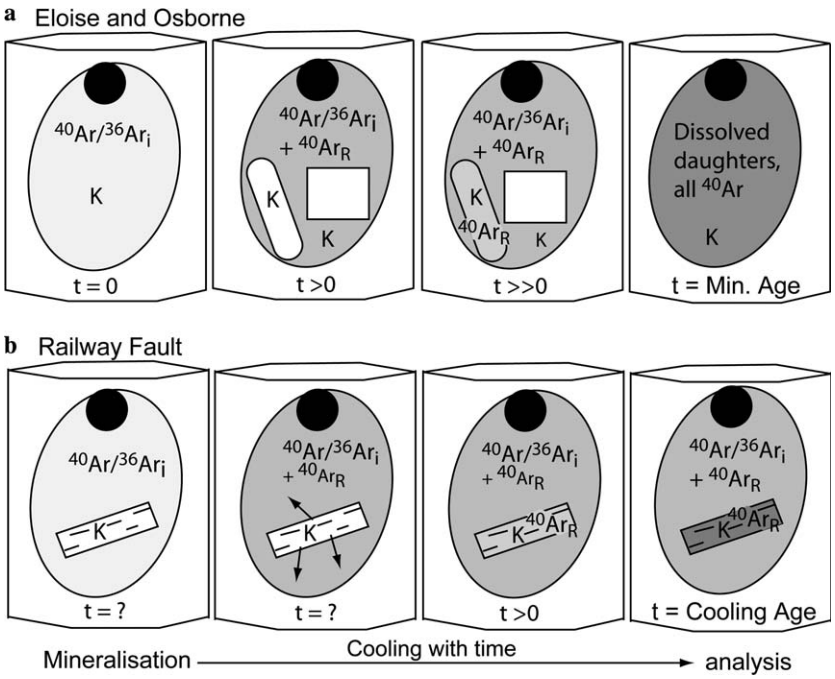

Fig. 8. Ar–Ar systematics of (a) quartz fluid inclusion ages and (b) quartz mineral impurity ages. The initial $^{40}Ar/^{36}Ar_i$ value at the time of mineralization is increased by in situ production of radiogenic $^{40}Ar_R$. The shading of the fluid inclusions and mineral impurities reflects the increasing concentration of $^{40}Ar_R$.

and Osborne is evaluated in Fig. 9 and is shown to be smaller than intra-sample variation in the initial $^{40}Ar/^{36}Ar$ value. In many cases the uncorrected measured $^{40}Ar/^{36}Ar$ value is within error of the corrected, initial $^{40}Ar/^{36}Ar$ value (Fig. 9a–d). This surprising result demonstrates that, in samples with similar Ar-concentrations, that do not contain K-mineral impurities (K/Cl values <1), uncertainties in the deposit age of 100's of Ma will be of little consequence in terms of determining the initial $^{40}Ar/^{36}Ar$ value. Furthermore, provided that mineral impurities are absent or minor in the sample the correction for $^{40}Ar_R$ will be unimportant.

In contrast the Railway Fault sample AW02-002, includes significant accidentally trapped mica (Fig. 2; K/Cl values $\gg$1). In this case the correction for post entrapment in situ production of radiogenic $^{40}Ar_R$ is large and the value determined is sensitive to the mineralization age used in the correction (Figs. 9e and f). A further implication of this is that intra-sample variation in the initial $^{40}Ar/^{36}Ar$ value cannot be determined reliably: Extraction of $^{39}Ar_K$ from sample AW02-002 is unrelated to the extraction of $^{38}Ar_{Cl}$ or $^{40}Ar_R$ (plus $^{40}Ar_E$) present in the fluid inclusions (Part I, Kendrick et al., 2006). As a result the correction for $^{40}Ar_R$ will be too small where $^{39}Ar_K$ is retained in the accidentally trapped mica and $^{40}Ar_R$ is extracted from fluid inclusions. The correction will be too large when $^{39}Ar_K$ and $^{40}Ar_R$-remaining in the mica are outgassed. The only way to overcome this problem is to calculate sample mean values that are presented in Figs. 9e and f. The mean corrected values for samples AW02-002a and AW02-002b, of 1921 and 730, are 22–24% lower than the uncorrected values (Fig. 9).

6. Perspective

6.1. Technique comparison

Ar–Ar age constraints on fluid inclusions that do not contain accidentally trapped mica or mineral impurities, in which fluid inclusions are the dominant reservoir of K (Osborne and Eloise) represent maximum ages of formation. Age constraints were difficult to obtain, for the samples in this study that include multiple fluid inclusion types, using either isochron diagrams or 3D ^{40}Ar–K–Cl–^{36}Ar plots. Mixing lines resulted in reduced precision (not accuracy) and regressions remained within error of the deposit ages.

In samples that contain accidentally trapped mica or mineral impurities, in vacuo crushing preferentially extracts inclusion fluids (Turner and Bannon, 1992; Kendrick et al., 2001a). Therefore, in vacuo crushing should yield fluid inclusion ages that represent the maximum age of formation. Where a homogenous population of fluid inclusion with uniform initial $^{40}Ar/^{36}Ar$ is present, robust isochrons can be obtained (Qiu, 1996; Qiu et al., 2002). The Tin–Tungsten and Gold related quartz samples dominated by fluid inclusions with atmospheric initial $^{40}Ar/^{36}Ar$ values (Qiu, 1996) and the Dongchuan copper quartz samples (Qiu et al., 2002) appear to represent examples of this phenomenon. However, $^{40}Ar_R$ loss from a mineral impurity into the surrounding fluid inclusion could elevate the apparent age of the fluid inclusions and because in vacuo crushing extracts $^{39}Ar_K$ from fluid inclusion only, the mineral impurity could remain undetected.

Subsequent stepped heating of the crushed residue has previously been applied to obtain gas from the solid-phase

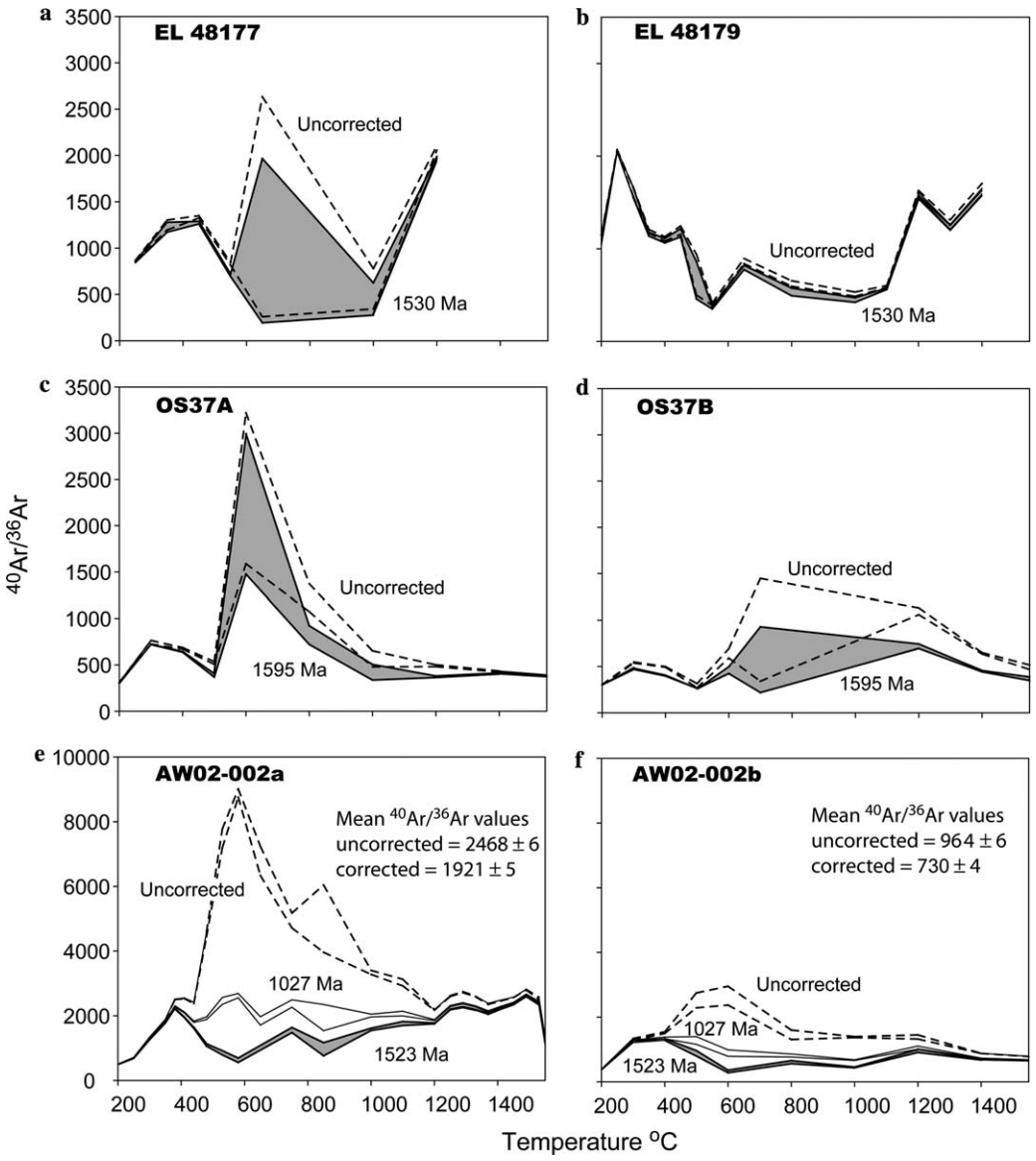

Fig. 9. $^{40}Ar/^{36}Ar$ values as a function of temperature for uncrushed samples analysed by stepped heating. The large uncertainty in the temperature range 600–800 °C is due to the low volume of gas released at these temperatures. (a and b) Eloise samples; (c and d) Osborne samples; (e and f) The Railway Fault samples have been corrected using the preferred 1523 Ma age of mineralization at Mt Isa, and the mineral impurity cooling age determined in Fig. 3.

impurities (Turner and Bannon, 1992; Kendrick et al., 2001a; Qiu et al., 2002). Resultant isochrons based primarily on the stepped heating data are therefore attributed to accidentally trapped mica and/or other mineral impurities and not the fluid inclusions themselves (Kelley et al., 1986; Kendrick et al., 2001a; Qiu et al., 2002). In many cases the mineral impurity ages may represent a cooling age rather than the formation age but in most rapidly cooled Phanerozoic magmatic-hydrothermal systems studied to date the cooling ages have been indistinguishable from the formation ages (e.g., Kelley et al., 1986; Kendrick et al., 2001a). However, apparent quartz ages that are up to 80 Ma younger than the age of associated granite intrusions in Cornwall (Turner and Bannon, 1992) could be re-interpreted as cooling ages rather than as indicating that mineralization post-dated granite intrusion by ~80 Ma.

Laser ablation quantitatively removes $^{38}Ar_{Cl}$ from daughter minerals (Kendrick et al., 2001a), but it is untested how efficiently $^{39}Ar_K$ or $^{40}Ar_R$ are removed from K-mineral impurities such as mica. If its effect is one of micro-crushing it would explain why it has provided only maximum ages of formation (Irwin and Roedder, 1995).

Laser heating of samples with a single generation of fluid inclusions has resulted in some good isochrons (McKee et al., 1993). However, laser heating could easily extract $^{39}Ar_K$ and $^{40}Ar_R$ from mineral impurities as well as the fluid inclusions. If unrecognized, an age obtained from a K-mineral sub-reservoir within fluid inclusions could provide an alternative explanation for younger than expected quartz ages in samples previously interpreted to contain only younger secondary fluid inclusions (McKee et al., 1993).

6.2. Recommendations and future directions

We have demonstrated that for a meaningful interpretation of quartz ages it is essential to understand the siting of K within the sample: if K is sited in fluid inclusions, resultant ages represent the maximum age of formation but are difficult to obtain; if K is sited in accidentally trapped mica, cooling ages can result. The optimum situation is probably K hosted by large mineral impurities within the quartz matrix.

Samples that require detailed investigation can be identified from mean K/Cl values of significantly greater than one (Table 2) and the degassing behaviour of $^{39}Ar_K$ relative to fluid inclusion hosted $^{38}Ar_{Cl}$ (Part I; Kendrick et al., 2006). Because the calculation of K and Cl from the noble gas proxies $^{38}Ar_{Cl}$ and $^{39}Ar_K$ provides a transparent method to assess the nature of impurities in quartz (e.g., Table 2) it should be considered an essential part of obtaining a 'quartz' age. The presence of optically invisible but abundant accidentally trapped-mica can then be confirmed by secondary electron microscopy (Fig. 2).

We have demonstrated that precision is obtainable at the 5% level even in samples with K-hosted in several different types of fluid inclusion, that do not contain K-mineral impurities, and for which true isochron regressions are difficult to obtain (Fig. 3). The Ar–Ar fluid inclusion ages currently support models with early ~1595 Ma syn-D_2 mineralisation at Osborne and are compatible with later 1514–1530 Ma D_3 mineralisation at Eloise. However, the major finding of this study is that the measured $^{40}Ar/^{36}Ar$ values of Proterozoic fluid inclusion are close to their initial values and, provided K-mineral impurities are absent, can in most cases be interpreted without any need for post-entrapment $^{40}Ar_R$ correction.

Acknowledgments

This work was funded by the Predictive Mineral Discovery Cooperative Research Centre (pmd*CRC) fluid history project (H4) and is published with permission. The work was made possible by sample donation from A. Wilde, T. Baker and R. Mustard. Isochron regressions have been performed utilizing Ken Ludwig's isoplot program. Stan Szczepanski is thanked for technical assistance in the lab. Chris Heinrich, Thomas Pettke and an anonymous GCA reviewer as well as the associate editor Bob Burrus are thanked for their constructive comments that helped improve the manuscript.

Associate editor: Robert C. Burruss

Appendix A. Argon data

Tabulated values are corrected for Ar-interference reactions and post-irradiation isotope decay

Temperature (°C)	^{40}Ar mol ($\times10^{-15}$)	^{36}Ar mol ($\times10^{-15}$)	Cl mol ($\times10^{-9}$)	K mol ($\times10^{-9}$)	% ^{39}Ar	Apparent age Ma
Eloise						
EL 48177 Combined crushing and stepped heating data (22.5 mg)						
Cr 1	28.0 ± 0.1	0.17 ± 0.01	1.29 ± 0.08			
Cr 2	2403.6 ± 2.4	2.46 ± 0.01	142.16 ± 9.23	6.19 ± 0.04	26.7	5620 ± 244
Cr 3	1065.3 ± 0.5	0.73 ± 0.01	78.92 ± 5.12	3.34 ± 0.02	41.1	5511 ± 278
200	140.31 ± 0.01	0.35 ± 0.01	18.0 ± 1.2			
300	240.3 ± 0.1	0.31 ± 0.01	14.0 ± 0.9	0.41 ± 0.01	42.9	6127 ± 1281
400	239.1 ± 0.2	0.39 ± 0.01	35.4 ± 2.3	1.14 ± 0.03	47.8	4063 ± 467
500	130.4 ± 0.2	0.135 ± 0.003	23.1 ± 1.5	1.88 ± 0.02	55.9	2840 ± 104
600	39.0 ± 0.4	0.224 ± 0.002	3.9 ± 0.3	1.75 ± 0.02	63.4	—
800	51.5 ± 0.1	0.02 ± 0.01	7.0 ± 0.5	2.1 ± 0.2	72.4	1793 ± 274
1000	67.08 ± 0.04	0.04 ± 0.01	5.5 ± 0.4	1.9 ± 0.2	80.7	2128 ± 428
1200	316.7 ± 0.7	0.42 ± 0.01	25.5 ± 1.7	1.6 ± 0.1	87.6	4252 ± 657
1400	823.7 ± 0.8	0.51 ± 0.01	60.9 ± 4.0	2.9 ± 0.1	100	5370 ± 1218
Total	5545 ± 3	5.76 ± 0.04	416 ± 12	23.2 ± 0.3	Fusion	4804 ± 282
EL 48177 Stepped heating data (26.0 mg)						
150	27.6 ± 0.1	0.14 ± 0.01	0.06 ± 0.01	0.17 ± 0.02	0.8	—
250	687.2 ± 0.5	0.79 ± 0.01	16.8 ± 1.1	1.04 ± 0.08	5.9	6442 ± 2273
350	884.0 ± 0.6	0.71 ± 0.03	54.2 ± 3.5	1.60 ± 0.04	13.7	6393 ± 1251
450	964.6 ± 0.6	0.72 ± 0.01	118.1 ± 7.7	4.15 ± 0.03	34.0	4931 ± 174
550	116.8 ± 0.1	0.141 ± 0.003	17.2 ± 1.1	1.60 ± 0.05	41.9	2808 ± 192
650	29.8 ± 0.1	0.02 ± 0.02	5.3 ± 0.3	0.70 ± 0.03	45.3	2360 ± 826
800	38.60 ± 0.02	0.14 ± 0.01	7.0 ± 0.5	1.52 ± 0.07	52.7	—
1000	72.7 ± 1.1	0.13 ± 0.05	6.0 ± 0.4	1.33 ± 0.07	59.2	2016 ± 1152
1200	1587.8 ± 1.1	0.76 ± 0.01	177.7 ± 11.5	8.34 ± 0.07	100	4760 ± 199
Total	4409 ± 2	3.56 ± 0.06	402 ± 14	20.4 ± 0.2	Fusion	4777 ± 218
EL 48179 Stepped heating data (92.0 mg)						
200	330.2 ± 0.1	0.30 ± 0.02	2.1 ± 0.1	0.32 ± 0.09	1.5	7412 ± 5164

(*continued on next page*)

Appendix Table (*continued*)

Temperature (°C)	^{40}Ar mol ($\times10^{-15}$)	^{36}Ar mol ($\times10^{-15}$)	Cl mol ($\times10^{-9}$)	K mol ($\times10^{-9}$)	% ^{39}Ar	Apparent age Ma
250	1249.3 ± 0.8	0.606 ± 0.004	12.9 ± 0.8	0.34 ± 0.07	3.2	9969 ± 7149
300	696.3 ± 0.3	0.43 ± 0.01	20.1 ± 1.3	0.38 ± 0.00	5.0	8655 ± 1416
350	385.60 ± 0.04	0.32 ± 0.01	22.0 ± 1.4	0.93 ± 0.06	9.4	5871 ± 1674
400	406.8 ± 0.3	0.37 ± 0.01	24.4 ± 1.6	0.64 ± 0.03	12.5	6568 ± 1973
450	496.6 ± 0.4	0.41 ± 0.02	29.0 ± 1.9	1.07 ± 0.06	17.7	6060 ± 1659
500	75.18 ± 0.01	0.10 ± 0.03	3.6 ± 0.2	0.58 ± 0.36	20.5	3523 ± 2892
550	39.2 ± 0.1	0.098 ± 0.003	1.8 ± 0.1	0.35 ± 0.07	22.2	2176 ± 762
650	55.7 ± 0.1	0.064 ± 0.002	2.4 ± 0.2	0.43 ± 0.03	24.2	3713 ± 803
800	84.89 ± 0.04	0.14 ± 0.01	4.9 ± 0.3	0.95 ± 0.05	28.8	2775 ± 502
1000	128.9 ± 0.1	0.26 ± 0.01	9.1 ± 0.6	1.39 ± 0.01	35.5	2530 ± 386
1100	208.5 ± 0.7	0.349 ± 0.004	13.2 ± 0.9	0.94 ± 0.01	40.0	4144 ± 212
1200	1400.0 ± 1.0	0.86 ± 0.01	112.7 ± 7.3	5.40 ± 0.05	65.9	5201 ± 247
1300	716.1 ± 0.4	0.56 ± 0.01	63.9 ± 4.1	3.29 ± 0.02	81.7	4805 ± 200
1400	894.8 ± 0.6	0.53 ± 0.01	78.0 ± 5.1	3.80 ± 0.05	100	5049 ± 353
Total	7168 ± 2	5.41 ± 0.05	400 ± 10	20.8 ± 0.4	Fusion	5601 ± 632
Osborne						
OS 37A Stepped heating data (41.9 mg)						
200	161.0 ± 0.2	0.52 ± 0.01	0.81 ± 0.05	0.19 ± 0.01	1.4	2475 ± 1340
300	188.2 ± 0.4	0.25 ± 0.01	5.2 ± 0.3	0.13 ± 0.03	2.4	7715 ± 5425
400	200.96 ± 0.02	0.296 ± 0.004	14.5 ± 0.9	0.89 ± 0.02	9.2	4343 ± 459
200	31.4 ± 0.1	0.060 ± 0.002	1.15 ± 0.08	0.76 ± 0.07	15.0	1595 ± 250
600	27.9 ± 0.1	0.012 ± 0.004	0.15 ± 0.02	0.17 ± 0.16	16.3	4506 ± 4339
800	36.9 ± 0.1	0.030 ± 0.004	0.45 ± 0.03	1.08 ± 0.08	24.5	2018 ± 284
1000	76.3 ± 7.6	0.13 ± 0.02	0.38 ± 0.03	1.75 ± 0.05	37.7	1764 ± 617
1200	149.6 ± 0.2	0.30 ± 0.01	1.92 ± 0.13	3.23 ± 0.04	62.3	1630 ± 89
1400	358.4 ± 0.2	0.84 ± 0.01	10.4 ± 0.7	1.56 ± 0.09	74.1	3422 ± 571
1600	804.7 ± 0.7	2.12 ± 0.01	11.7 ± 0.8	3.41 ± 0.06	100	2955 ± 198
Total	2035 ± 8	4.57 ± 0.03	47 ± 1	13.2 ± 0.2	Fusion	2952 ± 171
OS 37B Stepped heating data (43.2 mg)						
200	218.5 ± 0.8	0.718 ± 0.005	4.5 ± 0.3		0.0	—
300	212.2 ± 0.0	0.391 ± 0.005	25.8 ± 1.7	2.37 ± 0.01	7.9	2610 ± 89
400	154.6 ± 0.6	0.312 ± 0.003	33.0 ± 2.1	2.60 ± 0.04	16.6	1926 ± 72
500	36.5 ± 1.2	0.12 ± 0.01	0.8 ± 0.1	0.22 ± 0.04	17.3	—
600	72.5 ± 0.4	0.11 ± 0.01	12.9 ± 0.8	1.8 ± 0.1	23.4	1793 ± 235
700	17.1 ± 0.2	0.02 ± 0.01	0.8 ± 0.1	0.55 ± 0.03	25.2	1768 ± 752
800	18.6 ± 0.1		0.7 ± 0.0	0.67 ± 0.01	27.5	—
1000	20.1 ± 0.1	0.07 ± 0.01	1.7 ± 0.1	0.60 ± 0.11	29.5	—
1200	321.6 ± 0.0	0.29 ± 0.01	84.8 ± 5.5	9.9 ± 0.1	62.4	1914 ± 50
1400	209.5 ± 0.3	0.326 ± 0.004	40.0 ± 2.6	5.62 ± 0.03	81.2	1724 ± 35
1600	275.4 ± 0.3	0.62 ± 0.04	38.5 ± 2.5	5.7 ± 0.1	100	1496 ± 294
Total	1557 ± 2	2.99 ± 0.05	243.6 ± 7.2	30.0 ± 0.2	Fusion	1818 ± 68
Railway Fault						
AW02-002a Stepped heating data (126 mg)						
150	27.7 ± 0.1	0.10 ± 0.003	—	—		
200	456.5 ± 0.4	0.91 ± 0.01	0.64 ± 0.04	0.90 ± 0.04	0.0	5176 ± 1091
250	1427.6 ± 1.3	2.01 ± 0.02	3.0 ± 0.2	5.94 ± 0.05	0.3	4508 ± 190
300	2967.3 ± 2.9	2.23 ± 0.02	9.6 ± 0.6	15.6 ± 0.1	0.9	4594 ± 132
350	7352.7 ± 7.0	3.91 ± 0.03	29.9 ± 1.9	37.9 ± 0.3	2.3	4759 ± 155
380	3909.5 ± 3.0	1.56 ± 0.01	15.3 ± 1.0	40.7 ± 0.2	3.8	3692 ± 72
410	3716.9 ± 2.8	1.46 ± 0.01	11.4 ± 0.7	78.7 ± 0.5	6.8	2639 ± 36
440	3907.2 ± 3.1	1.63 ± 0.02	9.9 ± 0.6	116.0 ± 0.7	11.2	2180 ± 27
480	2305.7 ± 1.5	0.51 ± 0.01	2.1 ± 0.1	161.6 ± 1.0	17.3	1304 ± 12
530	2290.6 ± 1.7	0.31 ± 0.01	1.1 ± 0.1	187.7 ± 1.2	24.4	1188 ± 11
580	2022.6 ± 1.2	0.23 ± 0.00	0.66 ± 0.04	174.0 ± 1.1	31.0	1152 ± 10
650	1896.2 ± 1.2	0.28 ± 0.02	0.68 ± 0.04	168.7 ± 1.0	37.4	1115 ± 11
750	2746.2 ± 2.2	0.56 ± 0.03	2.7 ± 0.2	174.0 ± 1.0	44.0	1406 ± 14
850	1380.4 ± 0.2	0.28 ± 0.06	1.2 ± 0.1	103.0 ± 0.6	47.9	1252 ± 26
1000	2948.2 ± 2.4	0.88 ± 0.02	5.5 ± 0.4	143.7 ± 0.9	53.4	1644 ± 17
1100	3545.9 ± 3.2	1.17 ± 0.04	8.0 ± 0.5	137.2 ± 0.9	58.6	1892 ± 25
1200	11238.7 ± 9.5	5.15 ± 0.04	28.6 ± 1.9	198.7 ± 1.2	66.1	2863 ± 43

Appendix Table (*continued*)

Temperature (°C)	^{40}Ar mol ($\times10^{-15}$)	^{36}Ar mol ($\times10^{-15}$)	Cl mol ($\times10^{-9}$)	K mol ($\times10^{-9}$)	% ^{39}Ar	Apparent age Ma
1250	14282.0 ± 9.8	5.47 ± 0.04	39.1 ± 2.5	206.1 ± 1.2	73.9	3198 ± 53
1290	12847.1 ± 8.7	4.70 ± 0.04	34.0 ± 2.2	197.9 ± 1.2	81.4	3109 ± 51
1330	10912.9 ± 7.2	4.20 ± 0.03	27.0 ± 1.8	158.4 ± 1.0	87.4	3188 ± 53
1370	9613.4 ± 6.8	4.06 ± 0.04	22.7 ± 1.5	116.6 ± 0.7	91.8	3442 ± 62
1410	9143.2 ± 6.2	3.70 ± 0.03	20.1 ± 1.3	88.8 ± 0.5	95.2	3799 ± 79
1450	9020.0 ± 6.2	3.51 ± 0.02	17.5 ± 1.1	72.0 ± 0.4	97.9	4120 ± 97
1490	6065.7 ± 3.6	2.16 ± 0.01	10.9 ± 0.7	40.6 ± 0.3	99.4	4425 ± 117
1530	1960.0 ± 0.4	0.77 ± 0.01	3.6 ± 0.2	12.28 ± 0.08	99.9	4515 ± 133
1550	333.3 ± 0.2	0.27 ± 0.02	0.73 ± 0.05	2.29 ± 0.02	100	4128 ± 315
Total	128318 ± 24	52.0 ± 0.1	306 ± 5	2639 ± 4	Fusion	2674 ± 9
AW02-002b Combined crushing and stepped heating data (22.9 mg)						
Cr 1	132.5 ± 0.2	0.24 ± 0.03	0.53 ± 0.04	0.35 ± 0.03	0.1	4844 ± 2039
Cr 2	283.1 ± 0.1	0.51 ± 0.02	1.34 ± 0.10	0.94 ± 0.05	0.3	4499 ± 980
Cr 3	1163.8 ± 0.5	1.89 ± 0.01	4.3 ± 0.3	3.44 ± 0.05	1.1	4883 ± 343
Cr 4	2717.3 ± 1.9	2.93 ± 0.02	10.7 ± 0.7	7.69 ± 0.05	2.9	5418 ± 236
Cr 5	2767.4 ± 1.3	3.11 ± 0.02	10.3 ± 0.7	8.52 ± 0.05	4.9	5238 ± 203
Cr 6	1739.0 ± 0.5	1.81 ± 0.02	8.0 ± 0.5	6.46 ± 0.06	6.4	4983 ± 266
200	359.8 ± 0.3	1.01 ± 0.01	0.26 ± 0.03	2.69 ± 0.04	7.1	1853 ± 162
300	395.83 ± 0.03	0.65 ± 0.01	0.86 ± 0.06	8.91 ± 0.06	9.2	1866 ± 68
400	749.7 ± 0.3	0.64 ± 0.02	2.6 ± 0.2	34.9 ± 0.2	17.4	1482 ± 29
500	1587.4 ± 0.3	0.27 ± 0.01	0.71 ± 0.07	130.7 ± 1.0	48.1	1174 ± 12
600	784.3 ± 0.3	0.189 ± 0.002	0.14 ± 0.01	74.5 ± 0.5	65.6	1038 ± 9
800	451.20 ± 0.01	0.13 ± 0.03	0.36 ± 0.04	43.4 ± 0.3	75.8	1014 ± 28
1000	201.1 ± 0.2	0.196 ± 0.004	0.27 ± 0.02	15.7 ± 0.1	79.5	985 ± 14
1200	589.5 ± 0.6	0.67 ± 0.01	1.32 ± 0.09	23.8 ± 0.1	85.1	1511 ± 26
1400	2871.3 ± 3.6	3.57 ± 0.02	11.9 ± 0.8	45.4 ± 0.3	95.7	2581 ± 41
1600	2926.4 ± 2.1	5.78 ± 0.09	7.2 ± 0.5	18.2 ± 0.1	100	3329 ± 216
Total	19719 ± 5	23.6 ± 0.1	61 ± 1	425 ± 1	Fusion	2197 ± 17
AW02-002b Stepped heating data (23.3 mg)						
200	168.7 ± 0.1	0.44 ± 0.01	0.18 ± 0.01	0.67 ± 0.03	0.2	3136 ± 480
300	1206.6 ± 1.0	0.92 ± 0.02	3.6 ± 0.2	5.9 ± 0.1	1.9	4714 ± 277
400	1318.0 ± 0.7	0.87 ± 0.02	5.1 ± 0.3	16.9 ± 0.1	6.7	3227 ± 82
500	661.0 ± 0.2	0.26 ± 0.02	0.8 ± 0.1	39.8 ± 0.2	18.0	1394 ± 28
600	418.7 ± 0.3	0.16 ± 0.02	0.18 ± 0.04	34.1 ± 0.2	27.7	1127 ± 23
800	639 ± 64	0.439 ± 0.003	1.0 ± 0.1	34.4 ± 0.2	37.4	1402 ± 249
1000	161.8 ± 0.4	0.117 ± 0.001	0.24 ± 0.02	10.2 ± 0.1	40.3	1246 ± 15
1200	935.9 ± 1.0	0.68 ± 0.03	2.5 ± 0.2	27.1 ± 0.2	48.0	2076 ± 53
1400	5391.3 ± 6.0	6.13 ± 0.04	22.6 ± 1.5	113.7 ± 0.7	80.3	2261 ± 32
1600	4710.4 ± 3.8	6.24 ± 0.04	14.0 ± 0.9	69.2 ± 0.4	100	2628 ± 43
Total	15611 ± 64	16.2 ± 0.1	50 ± 2	352 ± 1	Fusion	2230 ± 30

References

Baker, T., 1998. Alternation, mineralisation and fluid evolution at the Eloise Cu–Au deposit, Cloncurry District, Northwest Queensland, Australia. *Econ. Geol.* **93**, 1213–1236.

Baker, T., Perkins, C., Blake, K.L., Williams, P.J., 2001. Radiogenic and stable isotope constraints on the genesis of the Eloise Cu–Au deposit, Cloncurry District, Northwest Queensland. *Econ. Geol.* **96**, 723–742.

Brannon, J.C., Podosek, F.A., McLimans, R.K., 1992. Alleghenian age of the Upper Mississippi Valley zinc-lead deposit determined by Rb–Sr dating of sphalerite. *Nature* **356**, 509–511.

Burnard, P., Graham, D., Turner, G., 1997. Vesicle-specific noble gas analyses of "popping rock; implications for primordial noble gases in the Earth. *Science* **276**, 568–571.

Carr, G.R., Denton, G.J., Parr, J., Sun, S., Korsch, M.J., Bodon, S.B., 2004. Lightning does strike twice: multiple ore events in major mineralised systems in northern Australia. SEG 2004: Predictive Mineral Discovery Under Cover, 27th September–1st October 2004. In: Muhling, J., Goldfarb, R., Vielreicher, N., Bierlein, F., Stumpfl, E., Groves, D.I., Kenworthy, S. (Eds.), *Centre for Global Metallogeny*, The University of Western Australia, Publication no., 33.

Coveney Jr., R.M., Ragan, V.M., Brannon, J.C., 2000. Temporal benchmarks for modeling Phanerozoic flow of basinal brines and hydrocarbons in the southern Midcontinent based on radiometrically dated calcite. *Geology* **28**, 795–798.

Darbyshire, D.P.F., Shepherd, T.J., 1985. Chronology of granite magmatism and associated mineralization, S.W. England. *J. Geol. Soc. London* **142**, 1159–1177.

Dodson, M.H., 1973. Closure temperature in cooling geochronological and petrological systems. *Contrib. Mineral. Petrol.* **40**, 259–274.

Gauthier, L., Hall, G., Stein, H., Schaltegger, U., 2001. The Osborne deposit, Cloncurry District: a 1595 Ma Cu–Au Skarn deposit. In: Williams, P.J. (Ed.), *A Hydrothermal Odyssey, Extended conference Abstracts*. James Cook University, Townesville, pp. 58–59.

Giles, D., Nutman, A.P., 2002. SHRIMP U-Pb monazite dating of 1600–1580 Ma amphibolite facies metamorphism in the southeastern Mt Isa block, Australia. *Aust. J. Earth Sci.* **49**, 455–465.

Hames, W.E., Bowring, S.A., 1994. An empirical evaluation of the argon diffusion geometry in muscovite. *Earth Planet. Sci. Lett.* **124**, 161–167.

Heinrich, C.A., Andrew, A.S., Wilkins, R.W.T., Patterson, D.J., 1989. A Fluid inclusion and stable isotope study of synmetamorphic copper ore formation at Mount Isa, Australia. *Econ. Geol.* **84**, 529–550.

Irwin, J.J., Roedder, E., 1995. Diverse origins of fluid inclusions at Bingham (Utah, USA), Butte (Montana, USA), St. Austell (Cornwall, UK) and Ascension Island (mid-Atlantic, UK), indicated by laser microprobe analysis of Cl, K, Br, I, Ba + Te, U, Ar, Kr, and Xe. *Geochim. Cosmochim. Acta* **59** (2), 295–312.

Kelley, S., Turner, G., Butterfield, A.W., Shepherd, T.J., 1986. The source and significance of argon isotopes in fluid inclusions from areas of mineralization. *Earth Plant. Sci. Lett.* **79**, 303–318.

Kendrick, M.A., Burgess, R., Pattrick, R.A.D., Turner, G., 2001a. Halogen and Ar–Ar age determinations of inclusions within quartz veins from porphyry copper deposits using complementary noble gas extraction techniques. *Chem. Geol.* **177**, 351–370.

Kendrick, M.A., Burgess, R., Pattrick, R.A.D., Turner, G., 2001b. Noble gas and halogen evidence on the origin of Cu-Porphyry mineralising fluids. *Geochim. Cosmochim. Acta* **65**, 2651–2668.

Kendrick, M.A., Miller, J.McL., Phillips, D., 2006. Part I. Decrepitation and Degassing Behaviour of Quartz up to 1560 °C: Analysis of Noble Gases and Halogens in Complex Fluid Inclusion Assemblages. *Geochim. Cosmochim Acta* **70**, 2540–2561.

Kent, A.J., McCuaig, T.C., 1997. Disturbed ^{40}Ar–^{39}Ar systematics in hydrothermal biotite and hornblende at the Scotia gold mine, Western Australia: evidence for argon loss associated with post-mineralisation fluid movement. *Geochim. Cosmochim. Acta* **61**, 4655–4669.

McDougall, I., Harrison, T.M., 1999. *Geochronology and Thermochronology by the $^{40}Ar/^{39}Ar$ Method*. Oxford University Press, Oxford, New York, p. 269.

McKee, E.H., Conrad, J.E., Turrin, B.D., Theodore, T.G., 1993. ^{40}Ar/^{39}Ar studies of fluid inclusions in vein quartz from battle mountain, Nevada. *USGS Bull.* **2039**, 155–165.

Nakai, S., Halliday, A.N., Kesler, S.E., Jones, H.D., 1990. Rb–Sr dating of sphalerites from Tennessee and the genesis of Mississippi Valley type ore deposits. *Nature* **346**, 354–357.

Nakai, S., Halliday, A.N., Kesler, S.E., Jones, H.D., Kyle, J.R., Lane, T.E., 1993. Rb–Sr dating of sphalerites from Mississippi valley-type (MVT) ore deposits. *Geochim. Cosmochim. Acta* **57**, 417–427.

Onstott, T.C., Miller, M.L., Ewing, R.C., Arnold, G.W., Walsh, D.S., 1995. Recoil refinements: implications for the ^{40}Ar/^{39}Ar dating technique. *Geochim. Cosmochim. Acta* **59**, 1821–1834.

Pettke, T., Diamond, L.W., 1995. Rb–Sr isotopic analysis of fluid inclusions in quartz: evaluation of bulk extraction procedures and geochronometer systematics using synthetic fluid inclusions. *Geochim. Cosmochim. Acta* **59**, 4009–4027.

Perkins, C., Wyborn, L.A.I., 1998. Age of Cu–Au mineralization, Cloncurry district, eastern Mt Isa Inlier, Queensland, as determined by 40Ar/39Ar dating. *Aust. J. Earth Sci.* **45**, 233–246.

Perkins, C., Heinrich, C.A., Wyborn, L.A.I., 1999. ^{40}Ar/^{39}Ar geochronology of copper mineralisation and regional alteration, Mount Isa, Australia. *Econ. Geol.* **94**, 23–36.

Phillips, D., Miller, J.McL., 2006. ^{40}Ar/^{39}Ar dating of mica-bearing pyrite from thermally overprinted Archaean gold deposits. *Geology* (in press).

Qiu, H-N., 1996. ^{40}Ar–^{39}Ar dating of the quartz samples from two mineral deposits in western Yunnan (SW China) by crushing in vacuum. *Chem. Geol.* **127**, 211–222.

Qiu, H-N., Zhu, B.Q., Sun, D.Z., 2002. Age significance interpreted from ^{40}Ar–^{39}Ar dating of quartz samples from the Dongchuan Copper Deposits, Yunnan, SW China, by crushing and heating. *Geochem. J.* **36**, 475–491.

Rama, S.N.I., Hart, S.R., Roedder, E., 1965. Excess radiogenic argon in fluid inclusions. *J. Geophys. Res.* **70**, 509–511.

Rubenach, M.J., Adshead, N., Oliver, N., Tullemans, F., Esser, D., Stein, H., 2001. The Osborne Cu–Au Deposit: geochronology and genesis of mineralization in relation to host albitites and irostones. In: Williams, P.J. (Ed.), *A Hydrothermal Odyssey, Extended conference Abstracts*. James Cook University, Townesville, pp. 172–173.

Shepherd, T.J., Darbyshire, D.P.F., 1981. Fluid inclusion Rb–Sr isochrons for dating mineral deposits. *Nature* **290**, 578–579.

Smith, P.E., Evensen, N.M., York, D., Szatmari, P., de Oliveira, D.C., 2001. Single crystal ^{40}Ar–^{39}Ar dating of pyrite: no fool's clock. *Geology* **29**, 403–406.

Spikings, R.A., Foster, D.A., Kohn, B.P., Lister, G.S., 2001. Post Orogenic (<1500 Ma) thermal History of the Proterozoic Eastern Fold Belt, Mount Isa Inlier, Australia. *Precambrian Res.* **109**, 103–144.

Spikings, R.A., Foster, D.A., Kohn, B.P., Lister, G.S., 2002. Post-orogenic (<1500 Ma) thermal history of the Palaeo-Mesoproterozoic, Mt. Isa province, NE Australia. *Tectonophysics* **349**, 327–365.

Swager, C.P., 1985. Syndeformational carbonate-replacement model for the copper mineralisation at mount Isa, Northwest Queensland: A Microstructural Study. *Econ. Geol.* **80**, 107–125.

Turner, G., Bannon, M.P., 1992. Argon isotope geochemistry of inclusion fluids from granite-associated mineral veins in southwest and northeast England. *Geochim. Cosmochim. Acta* **56**, 227–243.

Turner, G., Cadogan, P.H., 1974. Possible effects of ^{39}Ar recoil in ^{40}Ar–^{39}Ar dating. In: Proceedings of the 5th Lunar Science Conference, *Geochim. Cosmochim. Acta Suppl.* **5**, pp. 1601–1615.

York, D., Masiliwec, A., Kuybida, P., Hanes, J.A., Hall, C.M., Kenyon, W.J., Spooner, E.T.C., Scott, S.D., 1982. ^{40}Ar/^{39}Ar dating of pyrite. *Nature* **300**, 52–53.